# Identification of the Plant for Upright Stance in Humans: Multiple Movement Patterns From a Single Neural Strategy

**Article** *in* Journal of Neurophysiology · November 2008

DOI: 10.1152/jn.01272.2007 · Source: PubMed

CITATIONS
105

READS
347

**3 authors**, including:

Tim Kiemel
University of Maryland, College Park
**101** PUBLICATIONS **3,983** CITATIONS
SEE PROFILE

John Jeka
University of Delaware
**166** PUBLICATIONS **6,658** CITATIONS
SEE PROFILE

*J Neurophysiol* 100: 3394–3406, 2008.
First published October 1, 2008; doi:10.1152/jn.01272.2007.

# Identification of the Plant for Upright Stance in Humans: Multiple Movement Patterns From a Single Neural Strategy

**Tim Kiemel,[1] Alexander J. Elahi,[1] and John J. Jeka[1,2]**
[1]*Department of Kinesiology and* [2]*Program in Neuroscience and Cognitive Science, University of Maryland, College Park, Maryland*

Submitted 23 September 2008; accepted in final form 25 September 2008

**Kiemel T, Elahi AJ, Jeka JJ.** Identification of the plant for upright stance in humans: multiple movement patterns from a single neural strategy. *J Neurophysiol* 100: 3394–3406, 2008. First published October 1, 2008; doi:10.1152/jn.01272.2007. We determined properties of the plant during human upright stance using a closed-loop system identification method originally applied to human postural control by another group. To identify the plant, which was operationally defined as the mapping from muscle activation (rectified EMG signals) to body segment angles, we rotated the visual scene about the axis through the subject's ankles using a sum-of-sines stimulus signal. Because EMG signals from ankle muscles and from hip and lower trunk muscles showed similar responses to the visual perturbation across frequency, we combined EMG signals from all recorded muscles into a single plant input. Body kinematics were described by the trunk and leg angles in the sagittal plane. The phase responses of both angles to visual scene angle were similar at low frequencies and approached a difference of ~150° at higher frequencies. Therefore we considered leg and trunk angles as separate plant outputs. We modeled the plant with a two-joint (ankle and hip) model of the body, a second-order low-pass filter from EMG activity to active joint torques, and intrinsic stiffness and damping at both joints. The results indicated that the in-phase (ankle) pattern was neurally generated, whereas the out-of-phase pattern was caused by plant dynamics. Thus a single neural strategy leads to multiple kinematic patterns. Moreover, estimated intrinsic stiffness in the model was insufficient to stabilize the plant.

## INTRODUCTION

Studies of nonballistic motor actions that involve sensory feedback for ongoing corrections (i.e., a closed-loop feedback system) often attempt to determine how different components of the system contribute and interact in the overall behavior. For example, holding a cup while coffee is poured requires resistance of the limb to the added load so that the cup remains horizontal and coffee does not spill out. The source of this resistance has feedback (active) and intrinsic (passive) components. The feedback component is changes in force after some time delay because of changes in neural activation; the intrinsic component is instantaneous changes in force because of viscoelastic properties of the muscle (McMahon 1984), which may depend on the level of neural activation, but do not require changes in neural activation. Determining the relative contribution of these components is nontrivial, especially if the time delay associated with feedback is short compared with other time scales in the system.

A common method to address this problem is to "open the loop" so that the properties of different processes within the inherently closed-loop system can be studied in isolation to discern their influence on the behavior of interest (Leigh et al. 1982; Stark 1984). With regard to human motor control, this approach assumes that the system consists, in the simplest case, of two components: a plant and feedback. The plant being the entity being controlled along with its actuators (e.g., the body and its musculotendon actuators) and feedback being the changes in neural activation based on sensory information about the plant's behavior. A well-known example of this approach is the ingenious experiments with the pupillary reflex loop (Stark 1984). However, opening the loop is often criticized as a technique because the system is investigated under nonphysiological conditions and subjected to nonphysiological inputs. Moreover, opening the loop is not always possible, such as in the case of human postural control, because the plant alone is unstable. Remove all feedback and bipedal upright standing is no longer possible. In this study, we implement a closed-loop system identification method (van der Kooij et al. 2005) originally applied to human postural control by Fitzpatrick et al. (1996) to determine properties of the plant during human upright stance. We show how identifying the properties of the plant provides insight into a number of current issues.

From a control theory perspective, the postural control of upright stance in humans is a feedback control system consisting of two processes: the plant and feedback, as shown in Fig. 1 (Johansson et al. 1988; Kiemel et al. 2002; Kuo 1995, 2005; Masani et al. 2003; Peterka 2000; van der Kooij et al. 1999). Both of these processes are mappings from time-varying inputs to time-varying outputs. For purposes of this paper, we consider the plant to be the mapping from muscle activations to body segment angles, where we use rectified surface EMG signals as a proxy for muscle activations. (Our choice of body segment angles to describe the plant output is not essential; we could choose an equivalent coordinate system such as joint angles.) The plant is determined by properties of the body and the musculotendon actuators. Feedback is the mapping from body segment angles to muscle activations and is determined by properties of the sensory systems[1] and the nervous system.

The specific method of closed-loop system identification we use is the joint input-output method (van der Kooij et al. 2005). The method makes two assumptions. The first assumption is that the plant is linear. The body component of the plant (the mapping from joint torques to body segment angles) would be

[1] In control theory, sensors are often considered to be part of the plant (Özbay 2000). We do not do so here, because we are not able to measure sensory inputs to the nervous system

Address for reprint requests and other correspondence: T. Kiemel, Dept. of Kinesiology, College Park, MD 20742 (E-mail: kiemel@umd.edu).

The costs of publication of this article were defrayed in part by the payment of page charges. The article must therefore be hereby marked "*advertisement*" in accordance with 18 U.S.C. Section 1734 solely to indicate this fact.

  

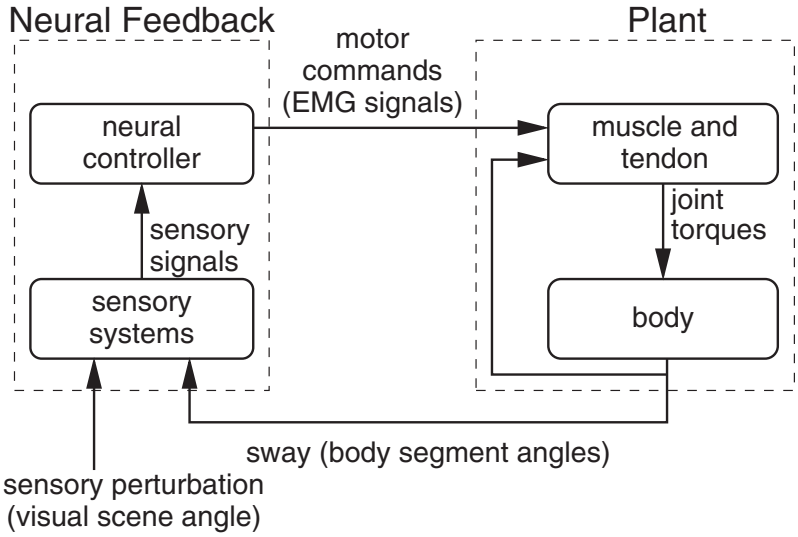


FIG. 1. Schematic representation of the postural control feedback loop. Signals used for the closed-loop system identification analysis are given in parentheses. The arrow from the body back to muscle and tendon represents the force-position and force-velocity properties of muscle, which we modeled using intrinsic stiffness and damping.

expected to be approximately linear, based on a small-angle approximation of a standard mechanical model of the body. Although the musculotendon component of the plant has well-known nonlinearities (McMahon 1984; Zajac 1989), it has often been approximated using linear models, with the proviso that model parameters depend on the conditions of the task (Genadry et al. 1988; Kearney et al. 1997). The second assumption of the method is that the plant can be considered to have a single input. Because a large number of muscles contribute to postural control, this assumption will only hold if the nervous system activates these muscles in a coordinated fashion such that all muscle activations are functions of a single control signal. In our study, we tested the single-input assumption by comparing the activities of muscles at the ankle with those acting at the hip or lower trunk.

Given a linear single-input multiple-output (SIMO) plant, the joint input-output method identifies the plant using a sensory perturbation. We used movement of the visual scene, whereas Fitzpatrick et al. (1996) used galvanic stimulation to perturb vestibular inputs. The effects of the sensory perturbation on the plant input (an EMG signal) and on the plant outputs (body segment angles) are each characterized by a frequency response function (FRF). The FRF characterizing the plant is computed as the perturbation-to-output FRF divided by the perturbation-to-input FRF (see METHODS).

In this study, our primary motivation to identify the plant was to investigate the mechanisms that determine its properties. We did this by using the identified plant FRF to fit parameters in a model of the plant. The model consisted of a two-joint (ankle and hip) inverted pendulum with a musculotendon actuator at each joint. Musculotendon properties are usually trivialized in posture models by assuming that joint torques directly follow motor commands, sometimes with a time delay. Even when musculotendon dynamics are included in a posture model (Kuo and Zajac 1993), they often contain some parameters that have not been measured during normal postural control of upright stance. By combining system identification with mechanistic modeling, we were able to estimate model parameters that were consistent with plant properties during standing. The resulting model allowed us to address two current controversies in postural control pertaining to multi-segment coordination and the contribution of intrinsic musculotendon stiffness to stability.

The multi-segment question pertains to recent studies based on a spectral analysis of postural sway during quiet stance showing the co-existence of in-phase and anti-phase phase relationships between the legs and trunk (Creath et al. 2005). At frequencies below ~1 Hz, the segments are in-phase, whereas at higher frequencies, they are antiphase, with a fairly abrupt shift between the two patterns. These two patterns resemble the "ankle and "hip" patterns observed during perturbed upright stance (Horak and Nashner 1986). The co-existence of these two patterns questions the prevailing notion that the ankle and hip patterns are always "selected" by the CNS to counteract the perturbation (Horak and Macpherson 1996). Recent evidence has suggested that the antiphase pattern during quiet stance rather than actively produced by the nervous system may instead be the result of biomechanics (Saffer et al. 2008; Zhang et al. 2007). The modeling results presented here support the view that biomechanics by itself can largely explain the antiphase pattern exhibited during unperturbed or weakly perturbed stance.

The second issue addressed by our approach is the current controversy about the contribution of intrinsic musculotendon stiffness to postural control. Winter et al. (1998) suggested that during the constrained conditions of unperturbed quiet stance, intrinsic muscle stiffness alone was capable of maintaining sway levels close to equilibrium. More recent studies argue that intrinsic stiffness is not sufficient by itself to stabilize upright stance (Casadio et al. 2005; Loram and Lakie 2002; Loram et al. 2007a,b; Morasso and Sanguineti 2002; Morasso and Schieppati 1999; Peterka 2002), meaning that the plant is unstable. However, there are widely varying estimates of the amount of stiffness. For example, Loram and Lakie (2002) estimated that mean intrinsic ankle stiffness was ~90% of that necessary to minimally counteract the torque produced by gravity assuming bending only at the ankle. In contrast, Peterka (2002) estimated intrinsic ankle stiffness to be smaller by about a factor of five. Our results lie between these two estimates. Potentially more important than estimating ankle intrinsic stiffness in isolation, our analysis considers intrinsic stiffness at both the ankle and hip joints, showing that a multi-joint

model is necessary to fully understand the contribution of intrinsic stiffness to postural control (Edwards 2007).

## METHODS

### *Experimental methods*

SUBJECTS. Eighteen subjects from the University of Maryland participated in the study. The results we present here exclude the data from one subject whose EMG responses differed qualitatively from those of other subjects (see *Signal processing*). Subjects ranged in age from 19 to 31 yr of age (mean: 22.7 ± 3.1 yr) and had no known musculoskeletal injuries or neurological disorders that might have affected their ability to maintain balance. All subjects were given both oral and written task instructions and gave written consent according to guidelines implemented by the Institutional Review Board at the University of Maryland before undergoing the experimental protocol.

EXPERIMENTAL SETUP. Each subject stood surrounded by three 305 × 244-cm rear-projected screens positioned at right angles to each other. The subject stood halfway between the left and right screens, facing the front screen at a distance of ~107 cm. To remove any effect of differences in participants' foot placements, an average preferred foot position of 11% of participant's height between heel centers and an eversion of the feet of 14° was used (McIlroy and Maki 1997). Subjects were instructed to maintain a comfortable upright stance, look straight ahead at the front screen, and not to focus on any particular triangle.

KINEMATICS. Body kinematics were measured using an OptoTrak (Northern Digital) system with a 120-Hz sampling rate. Markers were placed at the ankle (lateral malleolus), knee (lateral femoral condyle), hip (greater trochanter), and shoulder (acromion) on the right side of the subject's body.

EMG. Muscle activity was measured using a Noraxon Telemyo 900 surface EMG system. Pairs of Ag/AgCl electrodes (Ambu Blue Sensor M) with circular 154 $mm^2$ wet gel measuring areas were arranged parallel to the muscle fibers with an interelectrode distance of ~2 cm. Preamplifiers contained built-in 16- to 500-Hz band-pass filters and signals were digitized using a 1,020-Hz sampling rate. Activity was recorded from lateral gastrocnemius, soleus, tibialis anterior, rectus femoris, biceps femoris, erector spinae, and rectus abdominus muscles of the lumbar spine on the right side of the subject's body.

VIRTUAL VISUAL SCENE MOTION. CAVELib software (VRCO) was used to generate visual displays on the three screens surrounding the subject to simulate movement of a virtual rigid visual scene. The virtual scene consisted of three walls whose locations coincided with the locations of the screens when the scene was at rest. Each wall had 500 white 1.52 × 1.52 × 2.16-cm right triangles with random positions and orientations against a black background. For the front wall, triangles were excluded from a 30-cm-radius circle whose center was directly in front of the subject's eyes. The display on each screen was varied with time to simulate rotation of the visual scene about the axis through the subject's ankles, assuming a fixed perspective point at the average position of the subject's eyes. The visual scene angle was given by a sum-of-sines function of the form

$$v(t) = \sum_{j=1}^{10} (-1)^j A_j \sin(2\pi f_j t) \quad A_j = \begin{cases} A/f_j, & \text{if } j \le 8 \\ A/f_8, & \text{if } j > 8 \end{cases} \qquad (1)$$

where $t$ is time and the vector of 10 frequencies was $f$ = (3, 7, 13, 23, 43, 73, 113, 179, 263, 367)/125 in units of hertz. The frequencies varied from 0.024 to 2.936 Hz and were chosen as prime multiples of a base frequency (0.008 Hz) so that the visual motion repeated every 125 s while avoiding common low-order harmonics. Note that the amplitudes of the first eight sinusoids were scaled inversely with frequency, so that these sinusoids had the same peak velocity. The last two sinusoids had the same amplitude as the eighth sinusoid to improve detection of sway responses at the two highest frequencies compared with a previous study (Kiemel et al. 2006).

EXPERIMENTAL CONDITIONS. There were two conditions: a low-amplitude condition with $A = 0.02$ deg Hz in *Eq. 1* (peak-to-peak amplitude: 2.58 deg; peak velocity: 1.01 deg/s) and a high-amplitude condition with $A = 0.04$ deg Hz (peak-to-peak amplitude: 5.16 deg; peak velocity: 2.03 deg/s). There were five trials in each condition. The length of each trial was 250 s, allowing two repetitions of the visual motion stimulus. The order of the low- and high-amplitude trials was randomized.

### *Signal processing*

SIGNALS. The perturbation signal was the visual scene angle $v(t)$ from *Eq. 1*. The anterior-posterior and vertical positions of the ankle, hip, and shoulder markers were used to compute the leg angle $\theta_1(t)$ and the trunk angle $\theta_2(t)$ in the sagittal plane with respect to vertical. Positive angles indicated forward lean. For each of the seven recorded muscles, the mean was subtracted from the digitized EMG signal, and the signal was full-wave rectified. The rectified EMG signals were normalized by dividing by their root-mean-square values computed from all trials for the given subject, resulting in EMG signals $u_1(t)$, $u_2(t)$, ., $u_7(t)$. Because of subsequent signal processing described below, this initial normalization did not affect our final results. Because our frequency-domain analysis considered frequencies only ≤2.936 Hz, it was not necessary to low-pass filter the rectified EMG signals.

SPECTRAL ANALYSIS. For any two signals $x(t)$ and $y(t)$, the power spectral densities (PSDs) $p_{xx}(f)$ and $p_{yy}(f)$ and cross-spectral density $p_{xy}(f)$, where $f$ is frequency, were computed using Welch's method (Bendat and Piersol 2000) with 125-s Hanning windows and 50% overlap and averaged across the five trials for the given condition. Complex coherence is $c_{xy}(f) = p_{xy}(f)/\sqrt{p_{xx}(f)p_{yy}(f)}$ and (magnitude-squared) coherence is $|c_{xy}(f)|^2$. Coherence is a measure of the strength of the linear relationship between $x$ and $y$. Partial coherence between $x$ and $y$ adjusted for a third signal $z$ is

$$|c_{xy\cdot z}(f)|^2 = |p_{xy\cdot z}(f)|^2/p_{xx\cdot z}(f)p_{yy\cdot z}(f)$$

where $p_{xy\cdot z}(f) = p_{xy}(f) - p_{xz}(f)p_{zy}(f)/p_{zz}(f)$ is the conditional spectral density (Bendat and Piersol 2000). Partial coherence is a measure of the strength of the linear relationship between $x$ and $y$ that is not caused by their linear relationships with $z$.

The closed-loop frequency response function (FRF) from $x(t)$ to $y(t)$ is $H_{xy}(f) = p_{xy}(f)/p_{xx}(f)$. Gain is the absolute value of $H_{xy}(f)$ and phase is the argument of $H_{xy}(f)$, converted to degrees. A positive phase indicates that $y(t)$ was phase advanced relative to $x(t)$. We defined the mean FRF across subjects as $\bar{H}_{xy}(f) = \bar{c}_{xy}(f)\sqrt{\bar{p}_{yy}(f)/\bar{p}_{xx}(f)}$, where $\bar{c}_{xy}(f)$ is the mean complex coherence and $\bar{p}_{xx}(f)$ and $\bar{p}_{yy}(f)$ are the geometric mean PSDs. This definition of $H_{xy}(f)$, which reduces to $p_{xy}(f)/p_{xx}(f)$ in the case of a single subject, has an advantage if $y(t)$ is a normalized EMG signal. Specifically, if normalized EMG signals are obtained by multiplying the original signals $y_0(t)$ by a different scaling factor $\rho_i$ for each subject, $\bar{H}_{xy}(f) = \bar{\rho}H_{xy_0}(f)$, where $\bar{\rho}$ is the geometric mean of the scaling factors. Therefore normalization affects only overall gain but not phase or ratios between gains at different frequencies. Also, comparing our definition of $\bar{H}_{xy}(f)$ to the arithmetic mean, both means produced similar results when applied to the data in this study, but our definition of $\bar{H}_{xy}(f)$ tended to avoid large confidence intervals better than the arithmetic mean. When computing $\bar{H}_{xy}(f)$, we excluded data from one subject whose EMG responses did not follow the pattern of

the other 17 subjects. We computed bootstrap 95% CIs for the log gain and phase of $\bar{H}_{xy}(f)$, using the percentile-$t$ method with 4,000 bootstrap resamples and 400 nested bootstrap resamples for variance estimation (Hall 1988; Zoubir and Boashash 1998).

WEIGHTED EMG SIGNALS. Using the rectified EMG signals of the three ankle muscles (soleus, gastrocnemius, and tibialis anterior), we computed the weighted ankle EMG signal $u(t) = w_1u_1(t) + w_2u_2(t) + w_3u_3(t)$, where the weights $w_j$ were adjusted to maximize average coherence between the visual scene angle $v(t)$ and the weighted EMG signal $u(t)$ subject to the constraints $w_j \geq 0$ for posterior muscles, $w_j \leq 0$ for anterior muscles, and $|w_1| + |w_2| + |w_3| = 1$. Average coherence was computed by averaging complex coherence $c_{vu}$ across the two conditions and averaging coherence $|c_{vu}|^2$ across the 10 stimulus frequencies. The Matlab constrained optimization function FMINCON with user-supplied gradient was used to maximize coherence. We tried multiple sets of initial weights to increase the chance of finding the global maximum. We chose the sign convention that posterior muscles have positive weights for consistency with Fitzpatrick et al. (1996), who used the rectified soleus EMG signal for their analysis. For each subject, $u(t)$ was normalized by dividing by the geometric mean response amplitude across conditions and stimulus frequencies, where response amplitude is gain $H_{vu}(f)$ times stimulus amplitude. The same method was used to compute the weighted hip EMG signal from the EMG signals of the four muscles acting at the hip or lower trunk (rectus femoris, biceps femoris, erector spinae, and rectus abdominus) and to compute the weighted all-muscle EMG signal from all seven recorded EMG signals. To examine whether our results depended on the details of how we defined weighted EMG signals, we tested two other methods: weighting that maximized coherence but without constraints on the signs of the weights; and weighting with all weights of equal magnitude with positive and negative weights for posterior and anterior muscles, respectively.

### *Identification of the plant frequency response function*

We used the joint input-output method (van der Kooij et al. 2005) to identify the FRF of the plant. The key to the joint input-output method is that it identifies the plant using closed-loop responses of EMG and kinematic signals to a sensory perturbation, instead of the direct relationships among EMG and kinematic signals. Although spectral analsyis can show systematic patterns among EMG and kinematic signals (Saffer et al. 2008), it is not easy to disentangle the separate contributions of the plant and feedback to these patterns (van der Kooij et al. 2005).

To apply the joint input-output method, we assumed that the plant was linear and SIMO. The plant input, the control signal $u(t)$, was a weighted EMG signal. The plant outputs were the leg and trunk body segment angles $\theta_1(t)$ and $\theta_2(t)$, which were combined into the column vector $\boldsymbol{\theta}(t) = [\theta_1(t)\ \theta_2(t)]^T$ (T indicates transpose). Let $V(f)$, $U(f)$, and $\boldsymbol{\Theta}(f)$ be the Fourier transforms of $v(t)$, $u(t)$, and $\boldsymbol{\theta}(t)$. Then

$$\boldsymbol{\Theta}(f) = \mathbf{P}(f)U(f) + \mathbf{N}(f)$$

where $\mathbf{P}(f) = [P_1(f)\ P_2(f)]^T$ is the open-loop FRF of the SIMO plant and $\mathbf{N}(f)$ is the Fourier transform of a vector noise signal. Beause the visual scene angle was chosen by the experimenter, it was uncorrelated with the noise signal. Therefore

$$\mathbf{H}_{v\theta}(f) = \mathbf{P}(f)\mathbf{H}_{vu}(f) \quad (2)$$

where $\mathbf{H}_{v\boldsymbol{\theta}}(f) = [H_{v\theta_1}(f)\ H_{v\theta_2}(f)]^T$ is the vector closed-loop FRF from the visual scene angle to body segment angles and $H_{vu}(f)$ is the closed-loop FRF from the visual scene angle to the control signal. Rearranging *Eq. 2*, the plant FRF is $\mathbf{P}(f) = \mathbf{H}_{v\theta}(f)/H_{vu}(f)$. Following Fitzpatrick et al. (1996), we used mean closed-loop FRFs across subjects to identify the plant

$$\mathbf{P}(f) = \bar{\mathbf{H}}_{v\theta}(f)/\bar{H}_{vu}(f) \quad (3)$$

Mean FRFs were computed as described above. An alternative method would have to been to identify the plant for each subject and average across subjects. Our method reduced errors caused by subjects whose EMG signal $u(t)$ had low coherence with the visual scene angle $v(t)$. Confidence intervals for the log gain and phase of $\mathbf{P}(f)$ were computed using the bootstrap percentile-$t$ method (see *Signal processing*).

### *Model of plant*

The model of the plant consisted of a two-joint (ankle and hip) model of the body with synchronously activated ankle and hip lumped musculotendon actuators. Specifically, the mechanics of the body were described by a two-joint inverted pendulum in the sagittal plane with dynamics linearized about vertical

$$(J_1 + m_2l_1^2)\ddot{\theta}_1(t) + m_2l_1h_2\ddot{\theta}_2(t) - g(m_1h_1 + m_2l_1)\theta_1(t) = T_1(t) - T_2(t)$$

$$m_2l_1h_2\ddot{\theta}_1(t) + J_2\ddot{\theta}_2(t) - gm_2h_2\theta_2(t) = T_2(t) \quad (4)$$

*Equation 4* can be obtained from a standard three-joint model (Alexandrov et al. 2001) by removing one segment and linearizing about vertical. The input variables were the ankle torque $T_1(t)$ and the hip torque $T_2(t)$, where anterior muscles produce positive torque. The output variables were the leg segment angle $\theta_1(t)$ and the head, arms, and trunk (HAT) segment angle $\theta_2(t)$, where a positive angle indicates a forward lean with respect to vertical. The parameter $g$ was the acceleration caused by gravity. Anthropometric parameters for body segment $k$ ($k = 1$ for legs, $k = 2$ for HAT) were $m_k$, mass; $l_k$, length; $h_k$, height of the center of mass above the lower end of the segment; and $J_k$, the moment of inertia about the lower end of the segment.

Anthropometric parameters for the leg segment were computed by combining anthropometric parameters for shank and thigh segments: $m_1 = m_{1a} + m_{1b}$; $l_1 = l_{1a} + l_{1b}$; $h_1 = [m_{1a}h_{1a} + m_{1b}(l_{1a} + h_{1b})]/m_1$; and $J_1 = J_{1a} + J_{1b} + m_{1b}[(l_{1a} + h_{1b})^2 - h_{1b}^2]$, where subscripts 1a and 1b refer to the shank and thigh segments, respectively. Moments of inertia $J_k$ were expressed in terms of radii of gyration $r_k$: $J_k = m_kr_k^2$. Anthropometric parameters for the shank, thigh, and HAT segments are given in Table 1. Total body mass was the mean mass

TABLE 1. *Physical model parameters*

| Parameter Name | Symbol | Units | Value |
|---|---|---|---|
| Acceleration from gravity | $g$ | m/s$^2$ | 9.81 |
| Total subject mass | $m_{tot}$ | kg | 70.6 ± 15.1 |
| Shank segment length | $l_{1a}$ | m | 0.420 ± 0.028 |
| Thigh segment length | $l_{1b}$ | m | 0.378 ± 0.033 |
| HAT segment length | $l_2$ | m | 0.511 ± 0.036 |
| Shank relative mass | $m_{1a}/m_{tot}$ | | 0.093 |
| Thigh relative mass | $m_{1b}/m_{tot}$ | | 0.200 |
| HAT relative mass | $m_2/m_{tot}$ | | 0.678 |
| Shank relative COM position | $h_{1a}/l_{1a}$ | | 0.567 |
| Thigh relative COM position | $h_{1b}/l_{1b}$ | | 0.567 |
| HAT relative COM position | $h_2/l_2$ | | 0.626 |
| Shank relative radius of gyration | $r_{1a}/l_{1a}$ | | 0.643 |
| Thigh relative radius of gyration | $r_{1b}/l_{1b}$ | | 0.653 |
| HAT relative radius of gyration | $r_2/l_2$ | | 0.798 |

Total subject mass and segment lengths are given as mean ± SD. Parameters for the shank and thigh segments were used to compute parameters for the leg segment. COM positions and radii of gyration are defined relative to the lower end of each body segment. HAT, head, arms, and trunk; Com, center of mass.

of the subjects. Segment lengths were approximated by computing distances between the ankle, knee, hip, and shoulder markers in the sagittal plane and averaging across subjects. Other anthropometric parameters are from Winter (1990).

The musculotendon actuator for joint $j$ ($j = 1$ for ankle, $j = 2$ for hip) was modeled as

$$\ddot{T}_{0j}(t) + 2\omega_{0j}\eta_j\dot{T}_{0j}(t) + \omega_{0j}^2 T_{0j}(t) = -\gamma_j\omega_{0j}^2 u(t) \quad (5a)$$

$$T_j(t) = T_{0j}(t) - k_j\phi_j(t) - \alpha_j\dot{\phi}_j(t) \quad (5b)$$

where $\phi_1(t) = \theta_1(t)$ was the ankle angle, $\phi_2(t) = \theta_2(t) - \theta_1(t)$ was the hip angle, and the input control signal $u(t)$ was the same for both joints. The EMG-to-torque mapping from $u(t)$ to the active joint torque $T_{0j}(t)$ was modeled as a second-order low-pass filter with angular eigenfrequency $\omega_{0j}$, damping fraction $\eta_j$, and DC gain $\gamma_j$ (*Eq. 5a*; Genadry et al. 1988). The damping fraction $\eta_j$ indicates whether the filter is underdamped ($\eta_j < 1$) or overdamped ($\eta_j > 1$). The negative sign in the right side of *Eq. 5a* reflects our sign convention that $u(t) > 0$ corresponds to activation of posterior muscles. Total joint torque was the sum of active torque and passive torque is produced by intrinsic stiffness $k_j$ and intrinsic damping $\alpha_j$ (*Eq. 5b*; Peterka 2002).

The ten parameters $\omega_{01}$, $\omega_{02}$, $\eta_1$, $\eta_2$, $\gamma_1$, $\gamma_2$, $k_1$, $k_2$, $\alpha_1$, and $\alpha_2$ of the plant model were estimated based on the identified SIMO plant FRF from the weighted all-muscle EMG signal to the leg and trunk segment angles. The Matlab optimization toolbox was used to adjust parameters to minimize the objective function

$$\sum_{j=1}^{2}\sum_{k=1}^{10}|P_{0j}(f_k) - P_j(f_k)|^2/|P_j(f_k)|^2$$

where $\mathbf{P}(f) = [P_1(f)\ P_2(f)]^T$ is the identified plant FRF from *Eq. 3* and $\mathbf{P}_0(f) = [P_{01}(f)\ P_{02}(f)]^T$ is the FRF of the model. All model parameters were constrained to be non-negative. We tried multiple sets of initial parameters to increase the chance of finding the global minimum. Estimates of the parameters $\omega_{01}$, $\omega_{02}$, $\eta_1$, and $\eta_2$ do not depend on the assumed total mass $m_{tot}$; estimates of other parameters are proportional to $m_{tot}$. Because of our method of averaging FRFs across subjects, EMG normalization only affects the EMG-to-torque gains $\gamma_1$ and $\gamma_2$. Bootstrap SEs for model parameters were computed using 1,000 bootstrap resamples (Zoubir and Boashash 1998). Mean body mass and mean segment lengths were recomputed for each bootstrap resample.

The stability of the plant model was determined by converting the model to state-space form $\dot{\mathbf{y}}(t) = \mathbf{F}\mathbf{y}(t) + \mathbf{G}\mathbf{u}(t)$, where $y(t) = [\theta^1(t)\ \theta^2(t)\ \dot{\theta}^1(t)\ \dot{\theta}^2(t)\ T^{O1}(t)\ T^{O2}(t)\ \dot{T}^{O1}(t)\ \dot{T}^{O2}(t)]_T$ is the vector of state variables, $\mathbf{F}$ is an 8-by-8 matrix, and $\mathbf{G}$ is a 8-by-1 column vector. The plant is asymptotically stable if all the eigenvalues of $\mathbf{F}$ have negative real part. When the plant was unstable, we counted the number of instabilities as the number of eigenvalues with positive real part. Of the 10 estimated parameters, only the intrinsic joint parameters $k_1$, $k_2$, $\alpha_1$, and $\alpha_2$ affect stability. The EMG-to-torque parameters do not affect plant stability, because the EMG-to-torque mapping is always stable. If at least one of the intrinsic damping parameters $\alpha_1$ and $\alpha_2$ is positive, stability only depends on the intrinsic stiffness parameters $k_1$ and $k_2$. If hip intrinsic stiffness $k_2$ is very high, bending occurs only at the ankle and the criterion for stability is that ankle stiffness $k_1$ must exceed $mgh$, where $m = m_1 + m_2$ and $h = [m_1h_1 + m_2(l_1 + h_2)]/m$ are the mass and center-of-mass height of the combined leg and HAT segments. If ankle stiffness $k_1$ is very high, bending occurs only at the hip and the criterion for stability is that hip stiffness $k_2$ must exceed $m_2gh_2$.

## RESULTS

Example time series from one subject are shown in Fig. 2. We selected this example for illustrative purposes because the modulation of EMG activity was especially obvious for all three recorded ankle muscles, possibly because sway amplitude was unusually high. Slow forward and backward sway was correlated with the activity of the posterior muscles (soleus and gastrocnemius) and anterior muscle (tibialis anterior), respectively, as would be expected if muscles were activated to counteract the torque due to gravity. The last plot in Fig. 2 shows a weighted sum of the three EMG signals. The weights $w_j$ were selected to maximize the average coherence with the visual scene angle, subject to the constraint that $w_j \geq 0$ for posterior muscles and $w_j \leq 0$ for anterior muscles. Because the posterior and anterior weights had opposite signs, the weighted ankle EMG signal had both positive and negative values, being positive when the posterior muscles were primarily active and negative when the anterior muscle as primarily active. The mean weights across subjects were $0.41 \pm 0.20(1)$ (SD) for soleus, $0.46 \pm 0.22(0)$ for gastrocnemius, and $-0.13 \pm 0.17(3)$ for tibialis anterior, where the number of the 17 subjects with zero weights is given in parentheses. Note that although our weighting method allowed weights to be zero, this occurred infrequently. In addition to the weighted ankle EMG signal, we also computed a weighted hip EMG signal from the four EMG signals recorded from muscles acting at the hip or lower trunk and a weighted all-muscle EMG signal from all seven recorded EMG signals. Mean weights for the hip EMG signal were $-0.31 \pm 0.22(2)$ for rectus femoris, $0.27 \pm 0.23(4)$ for biceps femoris, $0.29 \pm 0.22(0)$ for erector spinae, and $-0.13 \pm 0.13(6)$ for rectus abdominus.

Figure 3*A* shows the average coherence across subjects between the visual scene angle and the rectified EMG signal of each of three recorded ankle muscles. At each of the 10 perturbation frequencies, coherence was highest for gastrocnemius and lowest for tibialis anterior. Also shown is the coherence between the visual perturbation and the weighted sum of the three EMG signals, where weights were adjusted for each subject to maximize coherence. As expected, coherence for the weighted sum was greater than for any individual muscle, although the increase in coherence compared with gastrocnemius was rather small.

Similarly, Fig. 3*B* shows the coherence between the visual scene angle and the rectified EMG signal of each of the four recorded muscle that act at the hip or lower trunk. Coherence was lowest for rectus abdominus at all frequencies; the EMG signal with the highest coherence varied with frequency. Taking the weighted sum of the individual EMG signals increased coherence compared with the highest coherence for any individual muscle, with the increase here being larger than for the ankle muscles. Also shown is the coherence between the visual scene angle and the weighted sum of all seven recorded muscles. The coherence of this weighted all-muscle EMG signal was substantially higher than the coherence of the weighted hip EMG signal, but only slightly higher than the coherence of the weighted ankle EMG signal (Fig. 3*A*).

Figure 3, *C* and *D,* shows the partial coherence between the visual scene angle and the EMG signals of individual muscles adjusted for the weighted all-muscle EMG signal. Partial coherence was low for all muscles and all frequencies, indi-

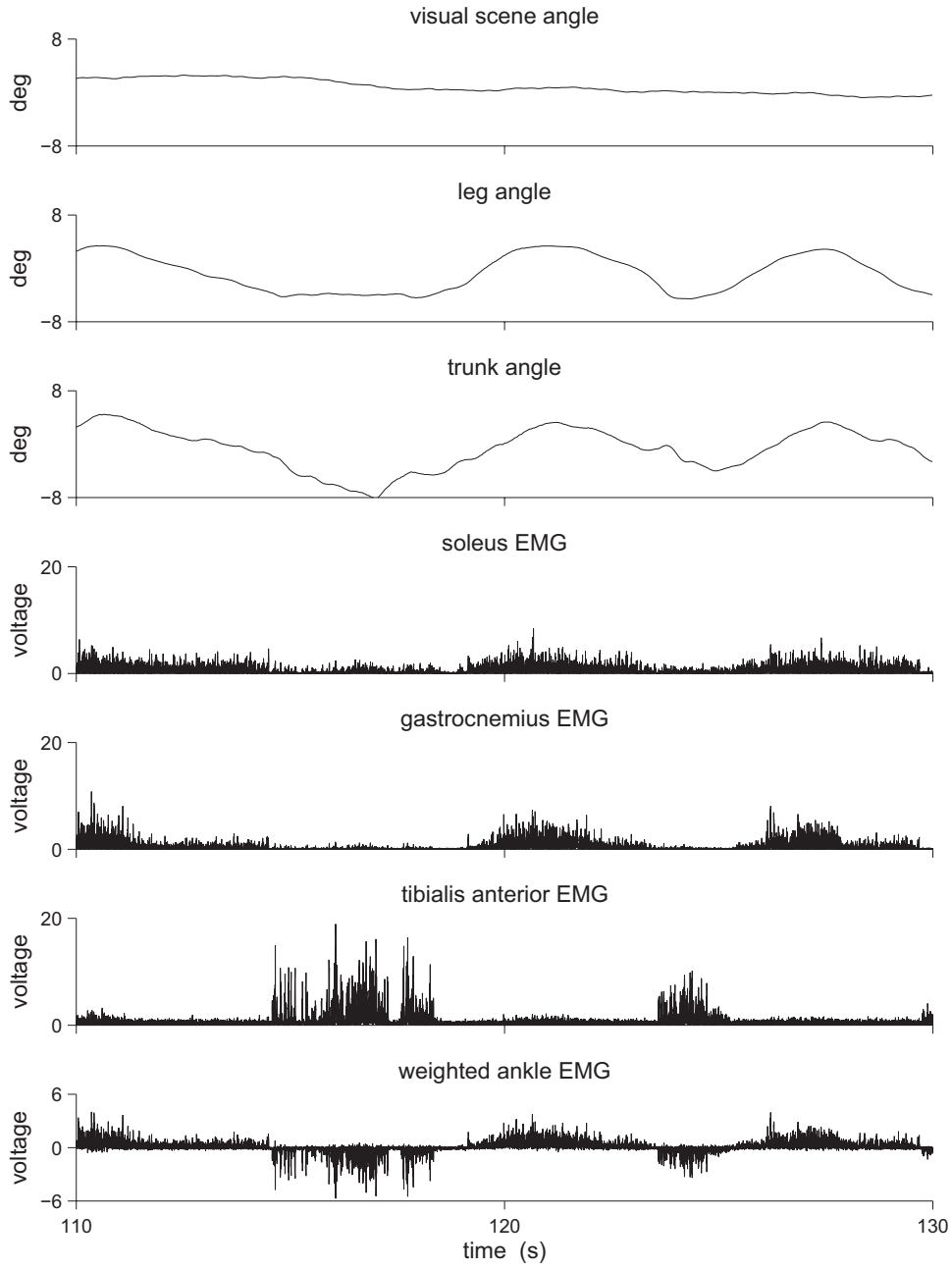


FIG. 2. Example time series from a subject in the high-amplitude condition. Mean values were subtracted from the visual scene, leg and trunk angles. EMG signals of individual muscles were normalized by dividing by the root-mean-square value. The weighted ankle EMG signal was computed as a weighted sum of the soleus, gastrocnemius, and tibialis anterior signals with weights 0.25, 0.40, and −0.35, respectively, which maximized the average coherence with the visual scene angle.

cating that most of the coherence shown in Fig. 3, *A* and *B,* between the visual perturbation signal and individual EMG signals can be explained by the linear relationships between each of these signals and the weighted all-muscle EMG signal. This result will be referred to below to support our use of the weighted all-muscle EMG signal to represent the plant input.

*Frequency response functions*

Figure 4, *A* and *B,* shows the closed-loop single-input single-output (SISO) FRF from visual scene angle to the weighted ankle EMG signal, and Fig. 4, *C* and *D*, shows the closed-loop SIMO FRF from the visual scene angle to the leg and trunk segment angles. Each FRF is shown for both amplitudes of visual scene motion. When visual scene motion was doubled from low- to high-amplitude, gains of the EMG and segment-angle responses decreased. For kinematic measures, similar decreases in gain have been observed in many studies (Kiemel et al. 2006; Peterka 2002; Peterka and Benolken 1995) and has been generally interpreted as indicating sensory reweighting. Except at the higher frequencies, the decrease in gain was roughly 50%, indicating that response amplitudes were similar in both conditions. Phases of the responses were similar for both amplitudes of visual scene motion. EMG and segment angle responses exhibited phase leads of about 50 deg at the lowest stimulus frequency (0.024 Hz), with phase lags at the higher frequencies. The phase lags were generally smallest for the EMG response and greatest for the leg-segment response.

Dividing the FRF from visual scene angle to body segments angles (Fig. 4, *C* and *D*) by the FRF from visual scene angle to

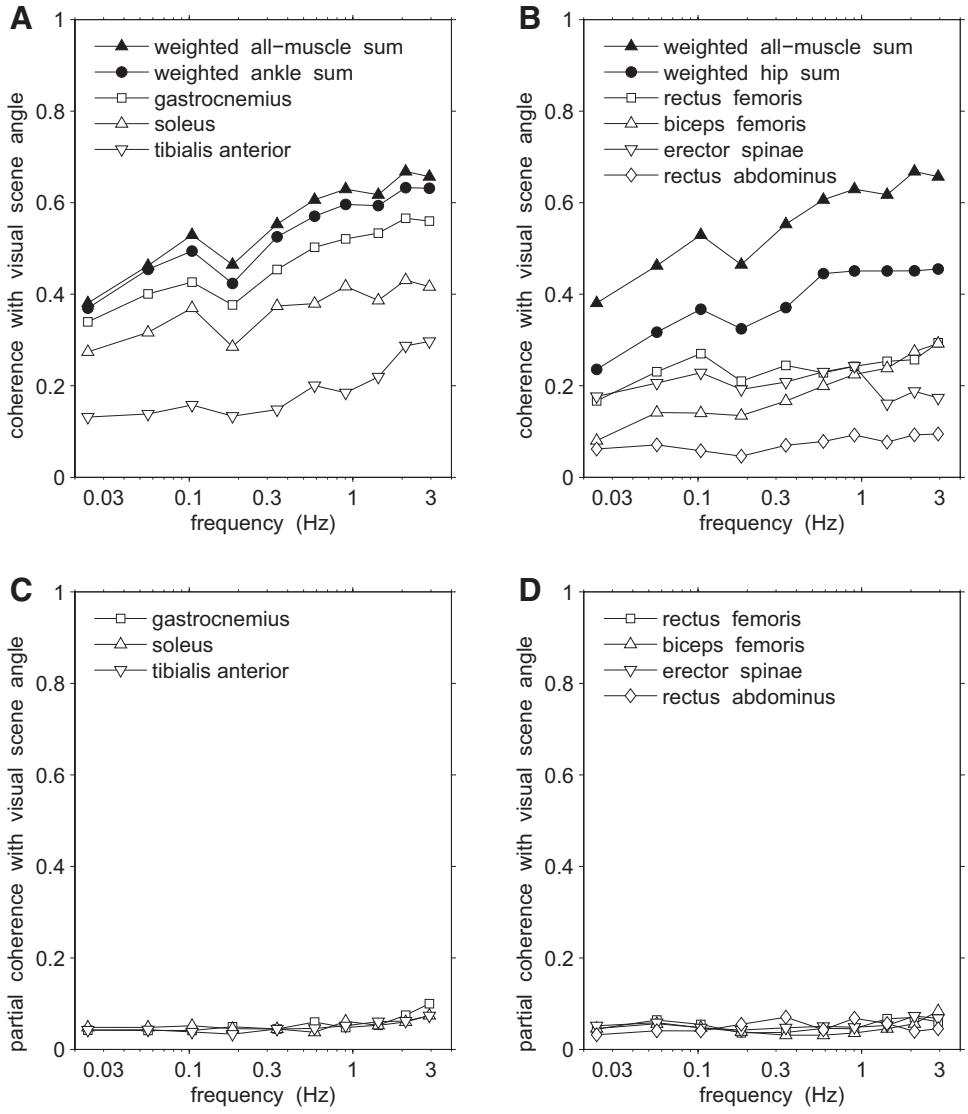


FIG. 3. Coherence and partial coherence between the visual scene angle and rectified EMG signals. *A*: coherence with ankle EMG signals. *B*: coherence with hip and lower trunk EMG signals. *C*: partial coherence with ankle EMG signals adjusted for the weighted all-muscle EMG signal. *D*: partial coherence with hip and lower trunk EMG signals adjusted for the weighted all-muscle EMG signal. Coherence was computed by averaging complex coherence $c_{vu}$ across both conditions and averaging coherence $|c_{vu}|^2$ across subjects. Partial coherence was averaged in the same way.

the EMG signal (Fig. 4, *A* and *B*) provided an estimate of the plant FRF (Fig. 4, *E* and *F*), that is, the open-loop SIMO FRF from the EMG signal to the body segment angles (see METHODS). This closed-loop identification of the plant FRF depends on the assumption that the plant can be approximated as having a single input. Note that the identified plant FRF is similar for the low- and high-amplitude conditions. This is consistent with the plant being linear. However, because EMG responses were similar for both conditions at most frequencies, our data do not provide a strong test of linearity. Gain was similar for both body segments at intermediate frequencies and was higher for the trunk segment at both low and high frequencies. The phase of both body segments were similar at low frequencies and gradually diverged with increasing frequency, with the leg segment showing a larger phase lag.

Figure 5, *A* and *B,* compares the responses of the weighted ankle and hip EMG signals to the visual scene angle. The ratio of the ankle and hip EMG gains remained roughly constant across frequency and the phase difference between the two EMG signals was close to zero. Although there was a significant phase lag of the ankle EMG at the two highest frequencies, the observed phase lag did not exceed 23 deg. Therefore to a first approximation, the ankle and hip EMG signals in response to the visual perturbation could be considered to be scaled versions of a single control signal. In contrast, recall from Fig. 4, *C* and *D*, that there were large differences in the responses of the leg and trunk body segment angles to the visual scene angle. These two responses are directly compared in Fig. 5, *C* and *D*. The gain ratio and phase difference of the leg and trunk responses showed a large dependence on frequency. In particular, the phase difference gradually varied from ~0 deg at low frequencies to a phase lag for the legs of ~150 deg at higher frequencies. The lag of the legs behind the trunk was significant at frequencies of 0.184 Hz and above. Thus, although it was possible to approximate the plant as having a single input, the kinematic output of the plant required multiple variables. In the terminology of control theory, the plant could be approximated as being SIMO, where the input is a weighted EMG signal and the outputs are the leg and trunk angles. In what follows, we used the weighted all-muscle EMG signal as the plant input when identifying the plant FRF. Further support for using the weighted all-muscle EMG signal to represent the coordinated activities of all muscles is our finding that the weighted all-muscle EMG signal explains most

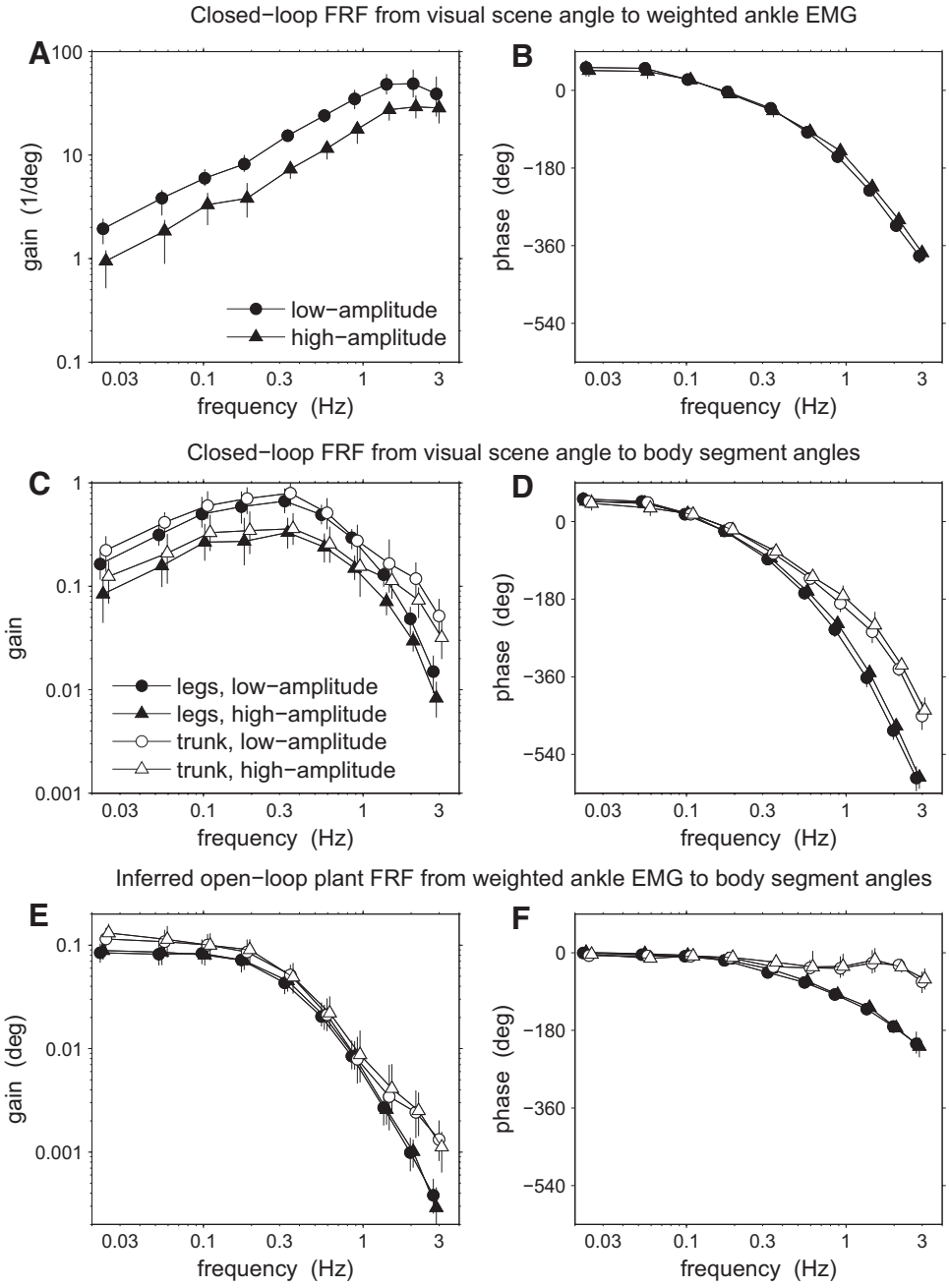


FIG. 4. Gain and phase of frequency response functions. The closed-loop frequency response functions (FRFs)(*A–B* and *C–D*) are means across subjects. The inferred open-loop plant FRF (*E–F*) was computed by dividing the FRF of *C–D* by the FRF of *A–B*. Gain of the plant in *E* equals the gain in *C* divided by the gain in *A*. Phase of the plant in *F* equals the phase in *D* minus the phase in *B*. FRFs are shown for both low- and high-amplitude visual scene motion. Errors bars indicate 95% bootstrap CIs.

of the coherence between the visual scene angle and the EMG signals of individual muscles (Fig. 3).

### *Estimation of parameters in model of plant*

We used the identified plant FRF to estimate musculotendon parameters in a SIMO model of the plant, assuming anthropometric parameters based on the subjects' mean mass and segments lengths (Tables 1 and 2; see METHODS). The control signal in the model, the single plant input, was assumed to synchronously activate ankle and hip actuators. For each actuator, the mapping from the control signal to active torque (the EMG-to-torque mapping) was a second-order low-pass filter. The total torque produced by each actuator was the sum of active torque, torque from intrinsic stiffness, and torque from intrinsic damping. Ankle and hip actuator torques were applied to a two-joint inverted pendulum model of the body with anthropometric parameters (Table 1).

Figure 6, *A* and *B,* compares the identified plant FRF (symbols) to the FRF of the fitted plant model (curves) for the high-amplitude condition. The identified plant FRF, which uses the weighted all-muscle EMG signal as the plant input, is similar to the identified plant FRF using the weighted ankle EMG signal as the plant input (Fig. 4, *E* and *F*), as would be expected given the similar responses of the weighted ankle and hip EMG signals to the visual scene angle (Fig. 5, *A* and *B*). The synchronous activation of the ankle and hip actuators in the model leads to different responses of the leg and trunk segments, closely matching the identified plant FRF. Gain for both segments is similar in the mid-range of frequencies, but

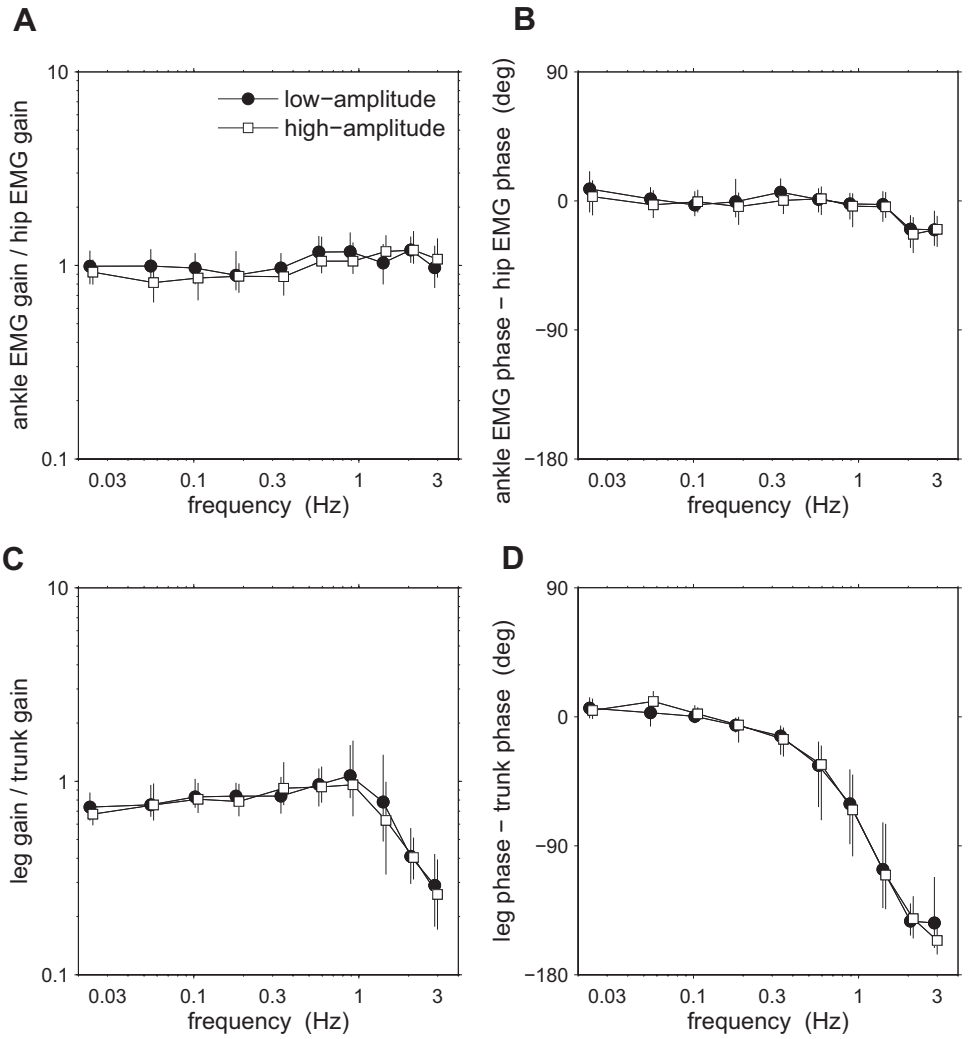


FIG. 5. Comparison of frequency response functions. *A* and *B*: comparison of the responses of the weighted ankle and hip EMG signals to the visual scene angle. *C* and *D*: comparison of the responses of the leg and trunk segment angles to the visual scene angle. Error bars indicate 95% bootstrap CIs.

higher for the trunk at both low and high frequencies. Phase for both segments is similar at low frequencies, with the trunk showing a phase lead with respect to the legs at higher frequencies.

Figure 6, *C* and *D*, shows the FRF of the model's EMG-to-torque mapping for each joint. Estimated eigenfrequencies ranged from ~6 to 9 rad/s (Table 2), resulting in substantial phase lags and decreases in gain at the higher stimulus frequencies. Estimated damping ratios ranged from ~1.0 (critically damped) to 1.6 (overdamped).

Figure 7 shows the fitted ankle and hip intrinsic stiffness values. We also show the region of stiffness values for which the plant is stable, the region for which the plant has one instability (one unstable eigenvalue), and the region for which the plant has two instabilities (two unstable eigenvalues). Stiffness values were similar for the low- and high-amplitude

TABLE 2. *Model parameters obtained by fitting model to identified plant FRF*

| Parameter Name | Symbol | Units | Low-Amplitude Condition | High-Amplitude Condition |
|---|---|---|---|---|
| EMG-to-torque parameters | | | | |
| Ankle eigenfrequency | $\omega_{01}$ | rad/s | 6.90 ± 0.98 | 7.64 ± 1.53 |
| Hip eigenfrequency | $\omega_{02}$ | rad/s | 9.46 ± 0.83 | 9.37 ± 0.95 |
| Ankle damping ratio | $\eta_1$ | | 1.03 ± 0.19 | 0.97 ± 0.31 |
| Hip damping ratio | $\eta_2$ | | 1.58 ± 0.17 | 1.50 ± 0.23 |
| Ankle DC gain | $\gamma_1$ | N m | 32.5 ± 6.5 | 27.4 ± 7.0 |
| Hip DC gain | $\gamma_2$ | N m | 14.1 ± 1.9 | 12.8 ± 2.1 |
| Intrinsic joint parameters | | | | |
| Ankle stiffness | $k_1$ | N m/rad | 293 ± 58 | 362 ± 66 |
| Hip stiffness | $k_2$ | N m/rad | 95 ± 28 | 147 ± 52 |
| Ankle damping | $\alpha_1$ | N m s/rad | 2.2 ± 11.4 | 0.0 ± 19.5 |
| Hip damping | $\alpha_2$ | N m s/rad | 27.4 ± 10.0 | 18.0 ± 11.6 |

Parameters values are given as estimate ± bootstrap SE. DC, direct current.

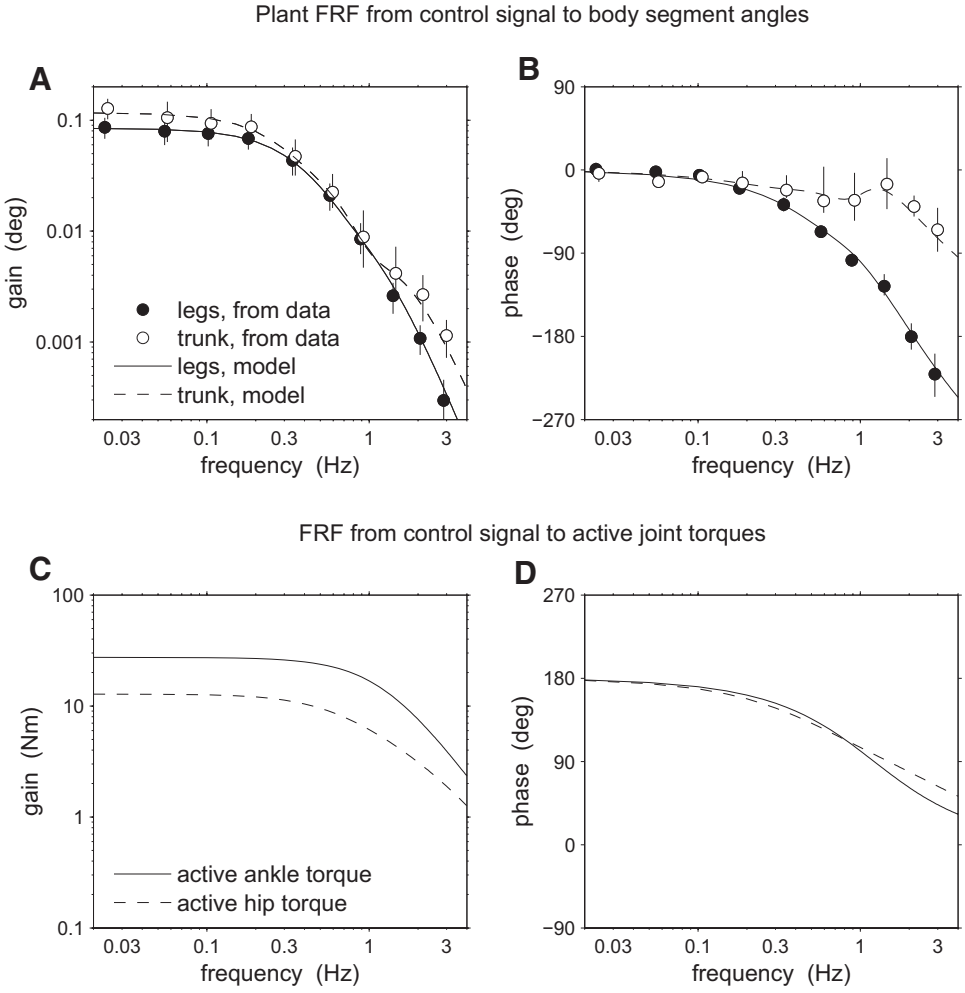


FIG. 6. Fitted model of the plant for the high-amplitude condition. The fitted model for the low-amplitude condition was similar. *A* and *B*: the empirical identified FRF of the single-input multiple-output (SIMO) plant (symbols) and the FRF of the fitted plant model (curves). For the empirical FRF, the weighted all-muscle EMG signal was used as the control signal. Error bars indicate 95% bootstrap CIs. *C* and *D*: the FRF from the control signal to active joint torques for the fitted plant model.

condition and were far from the region in which the plant is stable.

### *Robustness of results to different methods of weighting EMG signals*

The results above are based on weighted sums of EMG signals from multiple muscles. Weights $w_j$ were chosen to maximize coherence with the visual scene angle subject to the constraint that $w_j \geq 0$ for posterior muscles and $w_j \leq 0$ for anterior muscles. To examine whether our results depend on this particular method of choosing weights, we tested two other methods: weighting that maximized coherence but without constraints on the signs of the weights and weighting with all weights of equal magnitude with positive and negative weights for posterior and anterior muscles, respectively. These two alternative methods produced similar results to our primary method. In the vast majority of cases (397 of 400), gain and phases values produced by the alternative methods were within the confidence intervals of Figs. 4–6 for the primary method. In all cases, estimated model parameters using the alternative methods differed from the parameters for the primary method by less than the SEs given in Table 2. Note that the similarity of results for the three EMG weighting methods supports the view that all EMG signals, to a first approximation, reflect the same control signal. Under this view, the different methods of weighting EMG signals lead to different approximations of the same control signal and therefore produce similar results.

## DISCUSSION

In this study, we used a sensory perturbation to perform closed-loop system identification of the plant during postural control of upright stance. The basic method was similar to that used by Fitzpatrick et al. (1996), except that we extended the method in three respects. First, Fitzpatrick et al. identified an SISO plant with ankle angle as the only output, whereas we identified an SIMO plant with the leg and trunk angles as outputs. Second, Fitzpatrick et al. used only the soleus EMG signal as the plant input, whereas we used a weighted sum of the EMG signals from all seven recorded muscles as the plant input. We justified our use of this weighted all-muscle EMG signal by showing that weighted ankle and hip EMG signals showed similar responses to the visual scene angle. Third, we used movement of the visual scene to perturb visual inputs, whereas Fitzpatrick et al. used galvanic stimulation to perturb vestibular inputs. If the assumptions of the method are met (a linear plant with a single input), the choice of sensory perturbation should not affect the resulting identified plant. The leg component of our identified SIMO plant was similar to the SISO plant identified by Fitzpatrick et al., providing support for the validity of the method.

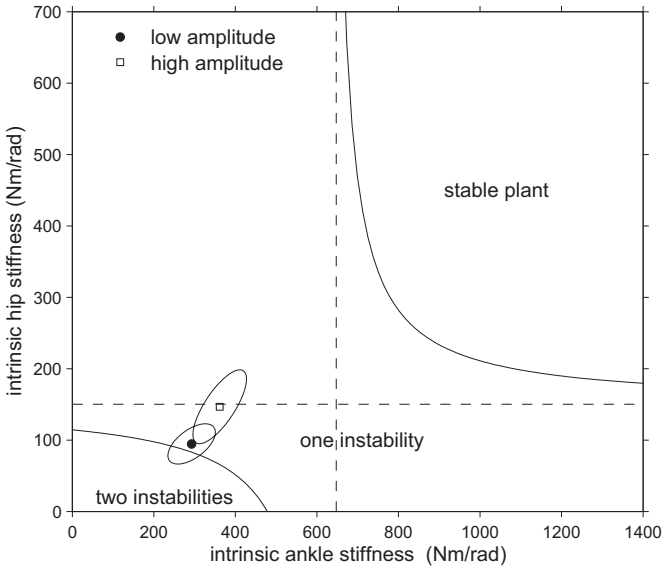


FIG. 7. Intrinsic ankle and hip stiffness of the fitted plant model. Ellipses indicate bootstrap SE. The vertical dashed line indicates *mgh*, the minimum intrinsic ankle stiffness necessary for stability assuming no movement at the hip. The horizontal dashed line indicates $m_2gh_2$, the minimum intrinsic hip stiffness necessary for stability assuming no movement at the ankle.

### *Multi-segment coordination*

The results are relevant to the issue of whether the multi-segment patterns (i.e., ankle and hip patterns) observed during upright stance reflect distinct neural strategies. Because the plant, as identified using a visual perturbation, is approximately single-input, the large differences in the leg and trunk phases in response to the visual perturbation cannot be caused by a neural strategy (Fig. 5). Instead these phase differences must be caused by the plant. This conclusion was shown by our plant model, which was able to reproduce the observed pattern of leg and trunk responses with synchronous ankle and hip muscle activation (Fig. 6).

Our single-input plant approximation is similar to a muscle synergy analysis in which the activation of a large number of muscles is approximated by the activation of a smaller number of muscle synergies (d'Avella and Bizzi 2005; Torres-Oviedo and Ting 2007). As defined by Torres-Oviedo and Ting, each muscle synergy is characterized by a vector of weights describing the contribution of each muscle. Each vector is multiplied by a time-varying activation coefficient, which is similar to our control signal. However, in a muscle synergy analysis, both the muscle weights and activation coefficients are required to be non-negative, whereas we allowed both the muscle weights and the control signal to be either positive or negative (Fig. 2). As a result, at least two muscle synergies, one for anterior muscles and one for posterior muscles, would be required to approximate the muscle activation pattern in our data. In fact, Torres-Oveido and Ting found that up to six muscle synergies were necessary to approximate EMG activities from 16 muscles on one side of the body when subjects were perturbed by platform translations. This relatively large number of synergies may be caused by their use of a strong platform perturbation with two spatial degrees of freedom compared with our weak sensory perturbation with only one spatial degree of freedom.

During quiet stance, the leg-trunk phase relationship also shows a transition from in-phase at lower frequencies to out-of-phase at higher frequencies, except that the transition is an abrupt change at ~1 Hz and the out-of-phase pattern is close to antiphase (Creath et al. 2005; Zhang et al. 2007), whereas here we observed a gradual transition with a phase lag of the legs behind the trunk that was first detectable at ~0.2 Hz and reached ~150 deg at 3 Hz. It is plausible that the phase pattern in quiet stance is also largely caused by the plant rather than a neural strategy. This hypothesis is supported by a spectral analysis of EMG activity during quiet stance (Saffer et al. 2008) that found a fixed phase relationship between hip EMG activity (biceps femoris) and ankle EMG activity (soleus and gastrocnemius) not only at low frequencies, where the in-phase pattern is observed, but also at higher frequencies where the antiphase trunk-leg pattern is observed. This previous study and this study indicate that the out-of-phase pattern during unperturbed or weakly perturbed stance is a function of plant dynamics rather than neural dynamics.

Unlike in this study, in which the leg-trunk phase was produced by a visual perturbation, the leg-trunk phase measured during quiet stance is produced by a variety of intrinsic perturbations, such as sensory noise and motor noise. This difference in how the postural system is perturbed presumably explains the difference in the leg-trunk phase pattern (a gradual transition here versus an abrupt transition during quiet stance). Modeling is necessary to study this question, which would require modeling the various noise sources in the system. Multi-segment posture models do exist (Alexandrov et al. 2005; Kuo 2005; van der Kooij et al. 1999); however, the behavior of these models have been primarily described in the time domain, rather than in the frequency domain. Moreover, these models have multiple control signals and therefore may not reproduce the nearly synchronous ankle and hip activation observed in this study.

### *Contribution of intrinsic stiffness to stability*

Our results are relevant to the current controversy concerning the level of intrinsic stiffness during upright stance (Casadio et al. 2005;Loram and Lakie 2002; Loram et al. 2007a,b; Morasso and Sanguineti 2002; Morasso and Schieppati 1999; Peterka 2002; Winter et al. 1998). Our fitted plant model shows a substantial amount of intrinsic stiffness at the ankle and hip joints, although this stiffness is far from the amount necessary to stabilize the plant (Fig. 7). Our estimates of intrinsic ankle stiffness of 293 and 362 N m/rad (Table 2), depending on condition, lie within the wide range of values from previous studies: ~90–120 N m/rad from Peterka (2002); 367 N m/rad from Casadio et al. (2005); and ~600 N m/rad from Loram and Lakie (2002).

The wide range of ankle stiffness estimates may indicate that a single value of stiffness cannot characterize intrinsic joint properties across a wide range of conditions (Zajac 1989). For example, linear Hill-type musculotendon models contain both series elastic and parallel elastic stiffness components (McMahon 1984), so that effective stiffness potentially depends on the frequency of joint angle changes. However, Loram et al. (2007b) argue that such frequency dependence is not relevant in the context of upright stance and instead emphasize the importance of nonlinear stiffness based on the finding of Loram et al. (2007a) that effective ankle stiffness decreases as the amplitude of joint movement increases. Loram et al. (2007a) estimate that a stiffness value of 67% of *mgh* is

appropriate for quiet stance, with lower values appropriate for perturbed stance. (Recall that *mgh* is the minimum stiffness necessary to stabilize the plant assuming bending only at the ankle.) Our estimates of intrinsic ankle stiffness are 45 and 56% of *mgh* (see Fig. 7) and therefore are roughly consistent with the estimate of Loram et al. (2007a) given that our estimates are based on weakly perturbed stance.

In this study, we analyzed the functional significance of ankle intrinsic stiffness in combination with hip intrinsic stiffness. Our estimates of intrinsic hip stiffness are, at most, roughly equal to the amount necessary to stabilize the plant, assuming no movement at the ankle (Fig. 7). For the plant to be robustly stable, both ankle and hip stiffness would need to increase. The dependence of stability on different joint stiffness values has been studied by Edwards (2007) for a three-joint model (ankle, knee, and hip). In general, if the stiffness of one joint in the model is decreased, the stiffness of other joints must be increased to maintain stability. Thus a single-joint model underestimates the amount of intrinsic ankle stiffness necessary for stability. Similarly, our two-joint model underestimates the amount of intrinsic ankle and hip stiffness necessary for stability because it ignores movement at other joints such as the knee. However, the amount of underestimation will be small if the stiffness values of other joints are high.

Our analysis of a multi-joint model of the plant also allowed us to address the question of how many instabilities of the body are stabilized by intrinsic stiffness, where we used the number of unstable eigenvalues to count instabilities. The number of instabilities of a multi-joint inverted pendulum equals the number of the joints. Each instability corresponds to an eigenmovment as defined by Alexandrov et al. (2001, 2005); a set of ratios between different body segment angles. Adding intrinsic stiffness (and some damping) to the joints can reduce the number of instabilities. Based on our estimates of ankle and hip intrinsic stiffness, we found that the plant is near the boundary between one and two instabilities (Fig. 7). Thus, although intrinsic stiffness is insufficient to stabilize the plant, it may be large enough to qualitatively change plant dynamics by reducing the number of instabilities inherent to a multi-joint body.

Our analysis of plant stability in this study (Fig. 7) assumed that there is some intrinsic damping at the ankle or hip joint. Our estimates of intrinsic ankle damping were $<3$ N m s/rad and less than their SE (Table 2), indicating that intrinsic ankle damping was too small to be detectable. Previous studies have also reported small values of intrinsic ankle damping with mean values of $<5$ N m s/rad (Casadio et al. 2005; Loram and Lakie 2002; Mirbagheri et al. 2000). Our estimates of intrinsic damping were larger for the hip (27.4 and 18.0 N m s/rad), suggesting that the hip joint rather than the ankle joint is the primary source of intrinsic damping.

### *EMG-to-torque model parameters*

A number of studies have estimated eigenfrequencies and damping ratios for the ankle EMG-to-torque mapping in humans. Because this mapping is nonlinear, estimated parameters based on a linear model will, in general, depend on operating conditions such as average ankle angle, average torque level, and the amount of torque modulation. For example, Genadry et al. (1988) found that the eigenfrequency for the triceps surae (soleus and gastrocnemius muscles) increased from ~8 to ~12 rad/s as the SD of torque modulation increased from 2.5 to 25% of maximum voluntary contraction. Our estimates of 6.90 and 7.64 rad/s for ankle-muscle eigenfrequency (Table 2) are similar to the lower end of this range, as would be expected because the modulation of ankle torque is low during weakly perturbed upright stance. Other studies have found somewhat higher eigenfrequencies. For example, Kearney et al. (1997) found that the eigenfrequency was ~20 rad/s for small ankle angle velocities. This difference in eigenfrequency estimates may be partially because of the fact that Kearney et al. (1997) included an electromechanical time delay in their EMG-to-torque model, whereas we and Genadry et al. (1988) did not. Electromechanical time delays have been measured during postural control (Müller and Redfern 2004), although there is some question whether these should be modeled as pure time delays (Corcos et al. 1992).

Our estimates of the ankle damping ratio for the EMG-to-torque mapping were about 1 (Table 2), indicating that the mapping is close to being critically damped. Previous studies have reported values in the range 0.5–1 for low modulation of ankle torque (Genadry et al. 1988) or small ankle angle velocities (Kearney et al. 1997).

### *Limitations of a single-input multijoint plant model*

In our study, using either ankle EMG or hip EMG as the plant input gave similar results, consistent with the hypothesis that the nervous system coordinates the activation of different muscles in such a way that the plant can be considered to have a single input. However, the similarity of ankle and hip EMG responses may be particular to using a visual perturbation. Testing the single-input hypothesis with other types of sensory perturbations would be informative. In particular, perturbing sensors in the lower body may show a different pattern of EMG responses than perturbing sensors in the head. Furthermore, the validity of the single-input assumption may depend on factors such as the amplitude of the perturbation. Our visual perturbation had a relatively small effect on the subjects' sway and EMG activities, suggesting that the control strategy used by the nervous system is probably similar to that used during unperturbed quiet stance. For discrete platform perturbations, it is known that the pattern of ankle versus hip EMG responses depends on factors such as the amplitude of the perturbation (Park et al. 2004), characteristics of the support surface (Horak and Nashner 1986), and neurological condition (Horak et al. 1990). The temporal shift in muscle activation from a distal-to-proximal pattern (i.e., ankle pattern) to a proximal-to-distal pattern (i.e., hip pattern) suggests a nonlinearity in multi-joint control that warrants further study with the techniques used in our study.

### *Conclusions*

Through a closed-loop system identification method, we showed that distinct patterns of behavior at the kinematic level do not necessarily reflect distinct neural strategies. Moreover, we have shown that such methods enable precise estimates of multi-link properties of the plant and how they contribute to the stabilization of upright stance. Although our plant model is highly simplified, it contains essential features of the process that the nervous system must control. Most importantly, the

plant is unstable. Because of internal (e.g., physiological tremor) and external (e.g., uneven support surface, moving visual environment) disturbances, the body is constantly correcting for deviations from vertical. Engineered devices, such as cars and robots, solve the stability problem by having a wide base of support and/or concentrating the bulk of its weight lower down. However, the human body has evolved with more than just upright stability as a constraint, with most of its mass concentrated higher up in the trunk, making it inherently unstable and prone to falls. These results are a step toward understanding the interplay between plant dynamics and the feedback processes that enable the functional advantages of bipedal upright stance.

## GRANTS

Funding for this research was provided by National Institute of Neurological Disorders and Stroke Grants R01 NS-46065 and R01 NS-35070 to J. J. Jeka.

## REFERENCES

**Alexandrov AV, Frolov AA, Horak FB, Carlson-Kuhta P, Park S.** Feedback equilibrium control during human standing. *Biol Cybern* 93: 309–322, 2005.

**Alexandrov AV, Frolov AA, Massion J.** Biomechanical analysis of movement strategies in human forward trunk bending. I. Modeling. *Biol Cybern* 84: 425–434, 2001.

**Bendat JS, Piersol AG.** *Random Data: Analysis and Measurement Procedures* (3rd ed.). New York: Wiley, 2000.

**Casadio M, Morasso PG, Sanguineti V.** Direct measurement of ankle stiffness during quiet standing: implications for control modelling and clinical application. *Gait Posture* 21: 410–424, 2005.

**Corcos DM, Gottlieb GL, Latash ML, Almeida GL, Agarwal GC.** Electromechanical delay: an experimental artifact. *J Electromyogr Kines* 2: 59–68, 1992.

**Creath R, Kiemel T, Horak F, Peterka R, Jeka J.** A unified view of quiet and perturbed stance: simultaneous co-existing excitable modes. *Neurosci Lett* 377: 75–80, 2005.

**d'Avella A, Bizzi E.** Shared and specific muscle synergies in natural motor behaviors. *Proc Natl Acad Sci USA* 102: 3076–3081, 2005.

**Edwards WT.** Effect of joint stiffness on standing stability. *Gait Posture* 25: 432–439, 2007.

**Fitzpatrick R, Burke D, Gandevia SC.** Loop gain of reflexes controlling human standing measured with the use of postural and vestibular disturbances. *J Neurophysiol* 76: 3994–4008, 1996.

**Genadry WF, Kearney RE, Hunter IW.** Dynamic relationship between EMG and torque at the human ankle: variation with contraction level and modulation. *Med Biol Eng Comput* 26: 489–496, 1988.

**Hall P.** Theoretical comparison of bootstrap confidence-intervals. *Ann Stat* 16: 927–953, 1988.

**Horak FB, Macpherson JM.** Postural orientation and equilibrium. In: *Exercise: Regulation and Integration of Multiple Systems,* edited by Rowell LB, Shepherd JT. New York: Oxford, 1996.

**Horak FB, Nashner LM.** Central programming of postural movements: adaptation to altered support-surface configurations. *J Neurophysiol* 55: 1369–1381, 1986.

**Horak FB, Nashner LM, Diener HC.** Postural strategies associated with somatosensory and vestibular loss. *Exp Brain Res* 82: 167–177, 1990.

**Johansson R, Magnusson M, Akesson M.** Identification of human postural dynamics. *IEEE Trans Biomed Eng* 35: 858–869, 1988.

**Kearney RE, Stein RB, Parameswaran L.** Identification of intrinsic and reflex contributions to human ankle stiffness dynamics. *IEEE Trans Biomed Eng* 44: 493–504, 1997.

**Kiemel T, Oie KS, Jeka JJ.** Multisensory fusion and the stochastic structure of postural sway. *Biol Cybern* 87: 262–277, 2002.

**Kiemel T, Oie KS, Jeka JJ.** Slow dynamics of postural sway are in the feedback loop. *J Neurophysiol* 95: 1410–1418, 2006.

**Kuo AD.** An optimal-control model for analyzing human postural balance. *IEEE Trans Biomed Eng* 42: 87–101, 1995.

**Kuo AD.** An optimal state estimation model of sensory integration in human postural balance. *J Neural Eng* 2: S235–S249, 2005.

**Kuo AD, Zajac FE.** Human standing posture: multi-joint movement strategies based on biomechanical constraints. *Prog Brain Res* 97: 349–358, 1993.

**Leigh RJ, Newman SA, Zee DS, Miller NR.** Visual following during stimulation of an immobile eye (the open loop condition). *Vision Res* 22: 1193–1197, 1982.

**Loram ID, Lakie M.** Direct measurement of human ankle stiffness during quiet standing: the intrinsic mechanical stiffness is insufficient for stability. *J Physiol* 545: 1041–1053, 2002.

**Loram ID, Maganaris CN, Lakie M.** The passive, human calf muscles in relation to standing: the non-linear decrease from short range to long range stiffness. *J Physiol* 584: 661–675, 2007a.

**Loram ID, Maganaris CN, Lakie M.** The passive, human calf muscles in relation to standing: the short range stiffness lies in the contractile component. *J Physiol* 584: 677–692, 2007b.

**Masani K, Popovic MR, Nakazawa K, Kouzaki M, Nozaki D.** Importance of body sway velocity information in controlling ankle extensor activities during quiet stance. *J Neurophysiol* 90: 3774–3782, 2003.

**McIlroy WE, Maki BE.** Preferred placement of the feet during quiet stance: development of a standardized foot placement for balance testing. *Clin Biomech* 12: 66–70, 1997.

**McMahon TA.** *Muscles, Reflexes, and Locomotion.* Princeton, NJ: Princeton University Press, 1984.

**Mirbagheri MM, Barbeau H, Kearney RE.** Intrinsic and reflex contributions to human ankle stiffness: variation with activation level and position. *Exp Brain Res* 135: 423–436, 2000.

**Morasso PG, Sanguineti V.** Ankle muscle stiffness alone cannot stabilize balance during quiet standing. *J Neurophysiol* 88: 2157–2162, 2002.

**Morasso PG, Schieppati M.** Can muscle stiffness alone stabilize upright standing? *J Neurophysiol* 82: 1622–1626, 1999.

**Müller MLTM, Redfern MS.** Correlation between EMG and COP onset latency in response to a horizontal platform translation. *J Biomech* 37: 1573–1581, 2004.

**Özbay H.** *Introduction to Feedback Control Theory*. Boca Raton, FL: CRC, 2000.

**Park S, Horak FB, Kuo AD.** Postural feedback responses scale with biomechanical constraints in human standing. *Exp Brain Res* 154: 417–427, 2004.

**Peterka RJ.** Postural control model interpretation of stabilogram diffusion analysis. *Biol Cybern* 82: 335–343, 2000.

**Peterka RJ.** Sensorimotor integration in human postural control. *J Neurophysiol* 88: 1097–1118, 2002.

**Peterka RJ, Benolken MS.** Role of somatosensory and vestibular cues in attenuating visually induced human postural sway. *Exp Brain Res* 105: 101–110, 1995.

**Saffer M, Kiemel T, Jeka J.** Coherence analysis of muscle activity during quiet stance. *Exp Brain Res* 185: 215–226, 2008.

**Stark LW.** The pupil as a paradigm for neurological control systems. *IEEE Trans Biomed Eng* 31: 919–924, 1984.

**Torres-Oviedo G, Ting LH.** Muscle synergies characterizing human postural responses. *J Neurophysiol* 98: 2144–2156, 2007.

**van der Kooij H, Jacobs R, Koopman B, Grootenboer H.** A multisensory integration model of human stance control. *Biol Cybern* 80: 299–308, 1999.

**van der Kooij H, Jacobs R, Koopman B, van der Helm F.** An adaptive model of sensory integration in a dynamic environment applied to human stance control. *Biol Cybern* 84: 103–115, 2001.

**van der Kooij H, van Asseldonk E, van der Helm FCT.** Comparison of different methods to identify and quantify balance control. *J Neurosci Methods* 145: 175–203, 2005.

**Winter DA.** *Biomechanics and Motor Control of Human Movement,* (2nd ed.). New York: Wiley-Interscience, 1990.

**Winter DA, Patla AE, Prince F, Gielo-Perczak K.** Stiffness control of balance in quiet standing. *J Neurophysiol* 80: 1211–1221, 1998.

**Zajac FE.** Muscle and tendon: properties, models, scaling, and applications to biomechanics and motor control. *Crit Rev Biomed Eng* 17: 359–411, 1989.

**Zhang Y, Kiemel T, Jeka J.** The influence of sensory information on two-component coordination during quiet stance. *Gait Posture* 26: 263–271, 2007.

**Zoubir AM, Boashash B.** The bootstrap and its application in signal processing. *IEEE Signal Proc Mag* 15: 56–76, 1998.